CrossMark

ORIGINAL ARTICLE

The metallogenic environment of the Dounan manganese deposit, Southeast Yunnan, China: evidence from geochemistry and Mössbauer spectroscopic

Jianbing Duan[1,3] · Yazhou Fu[1] · Zhengwei Zhang[1] · Xiangxian Ma[2] · Jiafei Xiao[1]

Abstract The Dounan manganese deposit is a typical large-scale marine sedimentary manganese deposit of the Middle Triassic in China. The metallogenic environment and change process directly dictate the migration, enrichment, and precipitation of Mn. To better understand its metallogenetic environment, a detailed study was undertaken involving field observation, mineralogical and geochemical and Mössbauer spectroscopic analyses. The major findings are as follows: (1) Lithofacies paleogeography, sedimentary structural characteristics, and geochemical indexes indicate that the deposits were formed in an epicontinental marine sedimentary basin environment of normal salinity; (2) there were three ore phases including Mn oxides, Mn carbonates, and mixed Mn ores. The ore minerals found were braunite, manganite, Ca-rhodochrosite, manganocalcite, and kutnahorite. Petrographic and mineralogical information indicates that the metallogenic environment was a weakly alkaline and weakly oxidized to weakly reduced environment, and the mineralization occurred near the redox interface; (3) the $V/(V + Ni)$ ratios, δCe and Fe^{2+}/Fe^{3+} found in profiles of Baigu and Gake ore sections show that the redox conditions of the ore-forming environment were continuously changing; and (4) three Fe species, $\alpha\text{-}Fe_2O_3$, $para\text{-}Fe^{3+}$, and $para\text{-}Fe^{2+}$, were found in hematite and clay mineral samples using Mössbauer spectrum analysis. The presence and distribution of these Fe species indicate that the deposit was formed in a typical sedimentary environment during the mineralization process. In summary, our study showed that redox was a key factor controlling the mineralization of the Dounan manganese deposit. Our results have led us to the conclusion that transgression and regression caused fluctuations in sea level, which in turn caused the change of the redox environment. Mössbauer spectroscopy is an effective tool for studying the redox conditions of the paleoenvironment in which sedimentary manganese deposits were formed.

1 Introduction

Southeast Yunnan Province is a region of high-quality manganese ore resources in southern China. The Dounan manganese ore belt is the most important high-quality manganese ore belt in the region, with many developed large- and medium-sized manganese deposits, such as Dounan, Laowu, Yanzijiao, and Daqing. Spatially, the metallogenic area is characterized by a small area and concentrated manganese deposits. The Dounan manganese deposit is a typical large marine sedimentary deposit (Wu and Zhu 1994; Huang et al. 1996). In the manganese-bearing rock series, there is separate manganese oxide and manganese carbonate mineral stratification. There are also two types of manganese minerals with mixed characteristics. Manganese nodules with oolitic, pisolitic, and

✉ Yazhou Fu
fuyazhou@mail.gyig.ac.cn

[1] State Key Laboratory of Ore Deposit Geochemistry, Institute of Geochemistry, Chinese Academy of Sciences, Guiyang 550081, China

[2] Key Laboratory of Petroleum Resources, Gansu Province; Key Laboratory of Petroleum Resources Research, Institute of Geology and Geophysics, Chinese Academy of Sciences, Lanzhou 730000, China

[3] University of Chinese Academy of Sciences, Beijing 101408, China

concentric zonal structures are commonly seen in the manganese ores of this deposit. These nodules are unique among China's manganese ore resources and have attracted the attention of numerous geologists.

Previous work on the Dounan manganese deposit has focused on sedimentary facies characteristics (Li et al. 2009; Xia et al. 2010), tectonics and mineralization (Bai et al. 2010), mineralogy (Hou 1994), and manganese source and genesis (Su 1983; Zhong 1986; Zheng and Zhang 1991; Du et al. 2013). However, the ore-controlling factors, migration and enrichment process of Mn, metallogenic environment and evolution, and metallogenic mechanism of the deposits remain poorly understood and controversial. Specifically, the metallogenic environment and evolution of the deposit are important in the study of the ore-forming mechanism of sedimentary manganese deposits, and directly dictate the migration, enrichment, and precipitation process of Mn. Using petrography, mineralogy, and sequence stratigraphy, Su (1983), Liu and Xue (1999), and Tang and Yi (2011) concluded that the Dounan manganese deposit was formed in a shallow-to-deep marine sedimentary basin environment via the use of petrography, mineralogy, and sequence stratigraphy. Change in the redox properties during sedimentary diagenesis is key mineralizing factors. Zheng and Zhang (1991), Luo and Du (1992), and Liu et al. (1988) considered that the deposit formed in a hydrothermal sedimentary environment via analysis of sedimentary facies and the geochemistry of major and trace elements. Due to the lack of the understanding of on the ore-forming environment, discussing the environmental conditions and the change processes in detail could lead to a new and significant understanding of the manganese mineralization process, metallogenic mechanism, and regularity of the Dounan manganese deposit and even the entire Dounan manganese ore belt.

Mössbauer spectroscopy is a powerful nuclear technique for characterizing the chemical states of iron. Iron exists in various chemical forms and oxidation states, and therefore can be used as an index to determine chemical changes that may occur in the environment and to elucidate their mechanisms. ^{57}Fe Mössbauer spectroscopy has frequently been used as a non-destructive analytical method to determine various Fe species in a variety of sedimentary samples (Hilton et al. 1986; Kubo et al. 1996; Zheng et al. 2001, 2010; Sun and Li 2017; Waander et al. 2017). In particular, the study of Fe speciation and Fe^{2+}/Fe^{3+} ratios in the vertical profile of sediments or ore beds can be used to indicate redox history and diagenesis processes (Kuno et al. 1998). This study analyzed the sedimentary environment and changes of the Dounan manganese deposit via systematic field survey, Mössbauer spectroscopy, mineralogy, and geochemistry in order to discern constraints on the manganese mineralization process.

2 Geological setting

The study area is on the western margin of the Yangtze plate in South China and is part of the depositional troughs of the Yunnan, Guizhou, and Guangxi provinces (Fig. 1a). The southern, western, and northern sides of the region, respectively, surround the Yuebei paleo-island, Ailaoshan uplift, and the Kangdian paleocontinent and Niushoushan paleo-island (Fig. 1b). Among them, the Yuebei paleo-island is composed of the manganese-bearing granitic gneiss and biotite schist of the Lower Devonian, and the Upper Devonian manganese-bearing limestone and siliceous rocks. The Kangdian paleocontinent is composed of iron-manganese slate in the Lower Cambrian Kunyang Group. The Ailaoshan uplift is composed of biotite plagioclase gneiss, amphibolite, marble, and other metamorphic rocks. The Permian Emeishan basalts are widely distributed on the ancient lands (Liu et al. 1984). According to paleogeographic features, ancient products containing manganese may have provided a large amount of manganese for the deposits through weathering and erosion. The early Indosinian tectonic movement caused the two sides of the Mingsu fault to disconnect, resulting in the side near the Yuebei paleo-island to rise and form a coast, and the other side dropped to form the Dounan Basin. Under the stable subsidence of the basin and several transgressions during the Latin period, a rock series bearing manganese deposited the element into the Dounan basin to a thickness of more than 800 m, constituting the main component of the Falang Formation. The area bounded by the Dounan Basin and the northern margin of the Yuebei paleo-island is the metallogenic manganese concentration zone that bears several manganese deposits, such as the Dounan, Laowu, and Daqing, and a series of manganese ore occurrences. Tectonically, the manganese deposits in the Dounan Basin are controlled mainly by the Dounan–Laowu curved syncline and an arc-shaped structure, which consist of the Wenma Fault trending in a northwest direction and the Mingsu fault in a northeast direction (Fig. 1b).

The manganese-bearing strata of the Dounan manganese ore belt are the Falang Formation (T_2f, Fig. 2a) of the Middle Triassic (Latin period), which forms a conformable contact with the Niaoge Formation of the Upper Triassic and an unconformable contact with the Gejiu Formation of the Middle Triassic. The lithological association is a set of shallow-marine mudstones, siltstones, and sandstones interbedded with carbonates and containing lamellibranchs, brachiopods, gastropods, alga, and other fossils (Liu and Xue 1999; Du et al. 2013). The Falang Formation is subdivided into six lithologic sections (T_2f_1–T_2f_6), including two main ore-bearing layers (T_2f_4 and T_2f_5) (Fig. 2). The
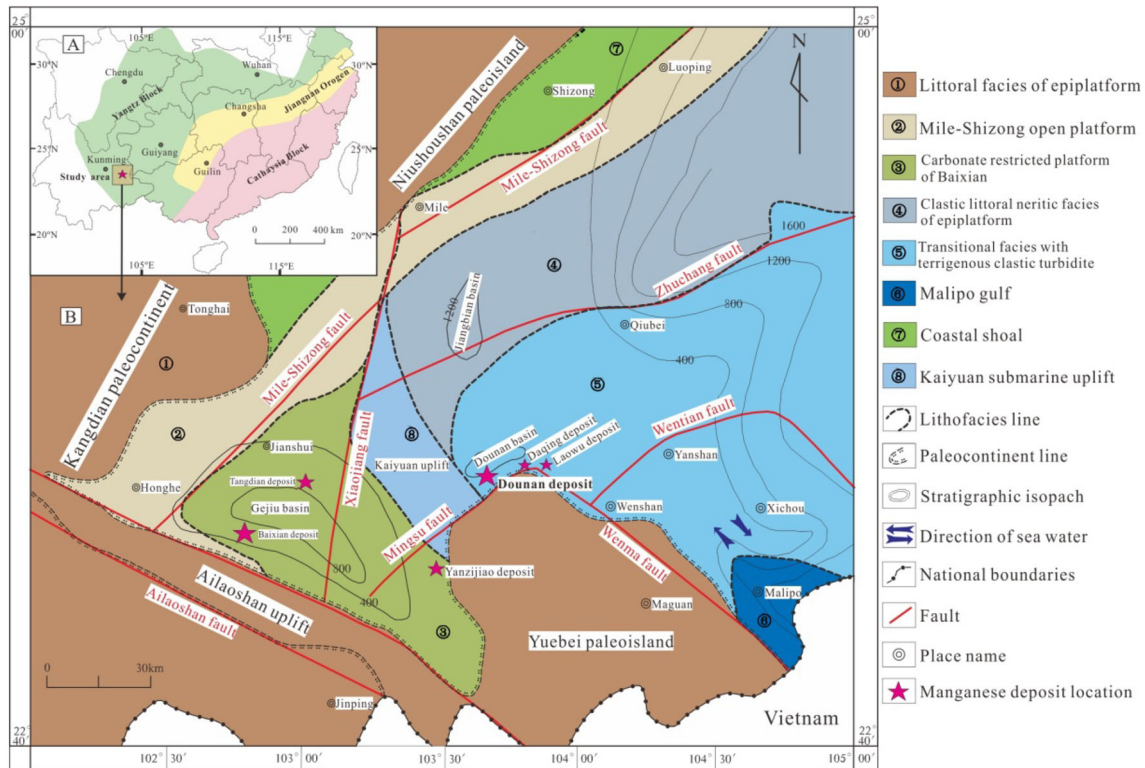
Fig. 1 **a** Tectonic map of Southern China and the location of the study area (Modified after Zhu et al. 2013); **b** the paleotectonic and paleogeography of Ladinic in southeastern Yunnan (Modified after Liu 1984; Hou et al. 1997)
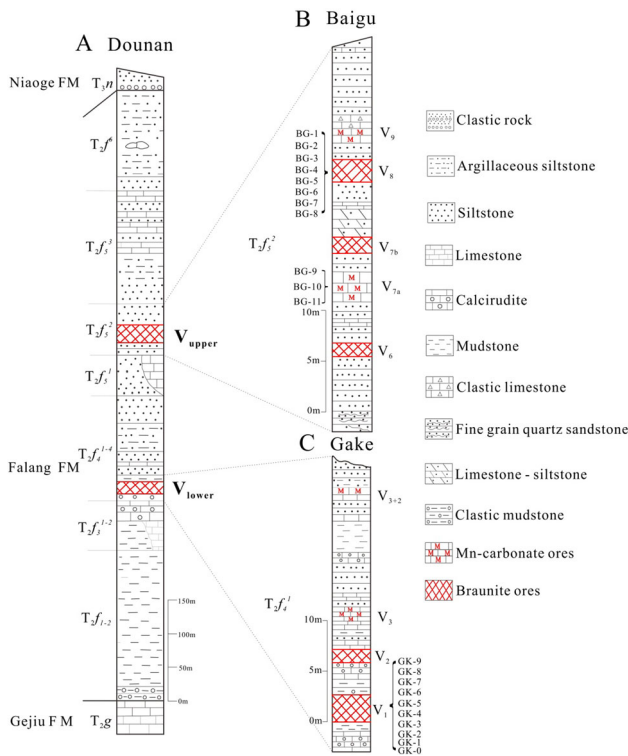

Fig. 2 Stratigraphic column of Dounan manganese deposit (Modified after Su 1983)

Dounan manganese deposit developed both the upper and lower ore beds.

3 Deposit characteristics

The Dounan Manganese deposit has a manganese resource of about 160 million tons. It extends westward from the Gake and eastward to the vicinity of Xinzhai, showing a large syncline (Fig. 3). According to the characteristics of the manganese-bearing rock series and geographical positions, the deposit is divided into two main ore-bearing layers ($T_2f_5^2$ and $T_2f_4^1$) (Fig. 2a) and five ore sections. The lower ore-bearing section Gake (Fig. 2c) and the upper section Baigu (Fig. 2b) are the main industrial sections.

The ore bodies are mostly layered, stratoid, and have lenticular morphology. There are many sedimentary structures like horizontal bedding, low-angle cross-bedding and current bedding developed in the ore beds. The types of manganese ores in different ore sections are very similar same and consist mainly of primary manganese ores (Liu et al. 1984). According to the composition, the primary manganese ores are classified as manganese oxide ore beds, manganese carbonate ore beds (Fig. 4a) as well as the mixture of the two (Fig. 4b). According to natural features, the ores can be divided into compact massive (Fig. 4b, c),

Fig. 3 Geological map of Dounan manganese deposit (Modified after Liu 1984)
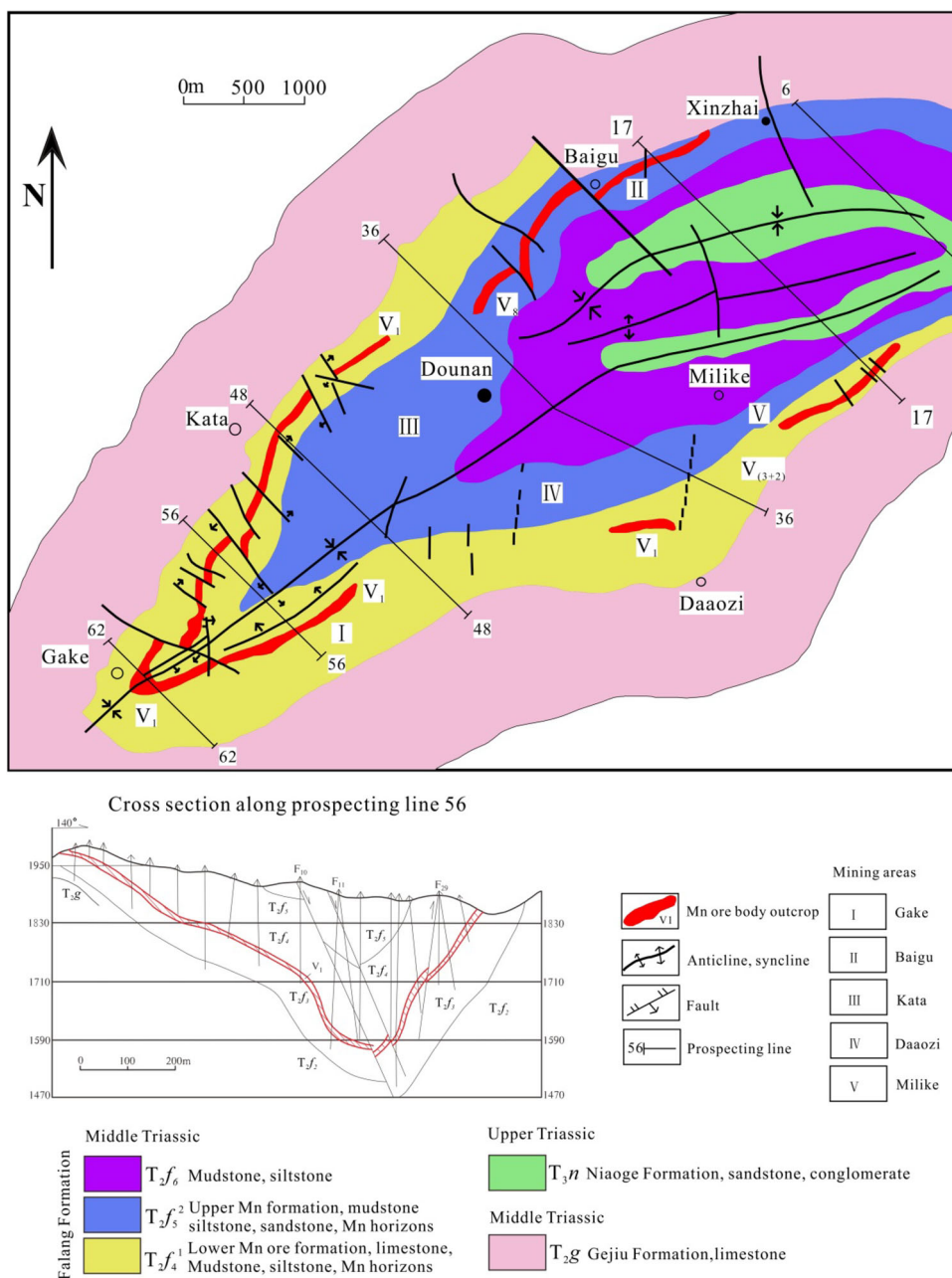
oolitic and pisolitic (Fig. 4f), and porphyritic types (Fig. 4e). The particle size of the oolitic and pisolitic ore is 0.5–6.0 mm, and the ore minerals are mainly manganese oxides or carbonates that form a ring-shaped with interbedded layers. The porphyritic manganese ore is characterized by the presence of purple-red manganese carbonate ore and black oxide ores that show a slight laminar structure. Among the mineral textures, the most common is oolitic (Fig. 4g), followed by the microgranular blastic texture of the manganese oxides (Fig. 4h) and the clastic texture commonly developed in the porphyritic

manganese ores (Fig. 4i). The gangue materials are mainly quartz, calcite, feldspar, and clay minerals.

4 Samples and analytical methods

The 21 samples investigated in the study were collected from the V_1 ore bed in the Gake, V_7 and V_8 ore beds in Baigu, respectively, (Fig. 2, Table 1), which are the lower and upper Mn-bearing series of the Falang Group in the Dounan manganese deposit. The sampling method was a continuous sampling of vertical profiles. Ten samples were
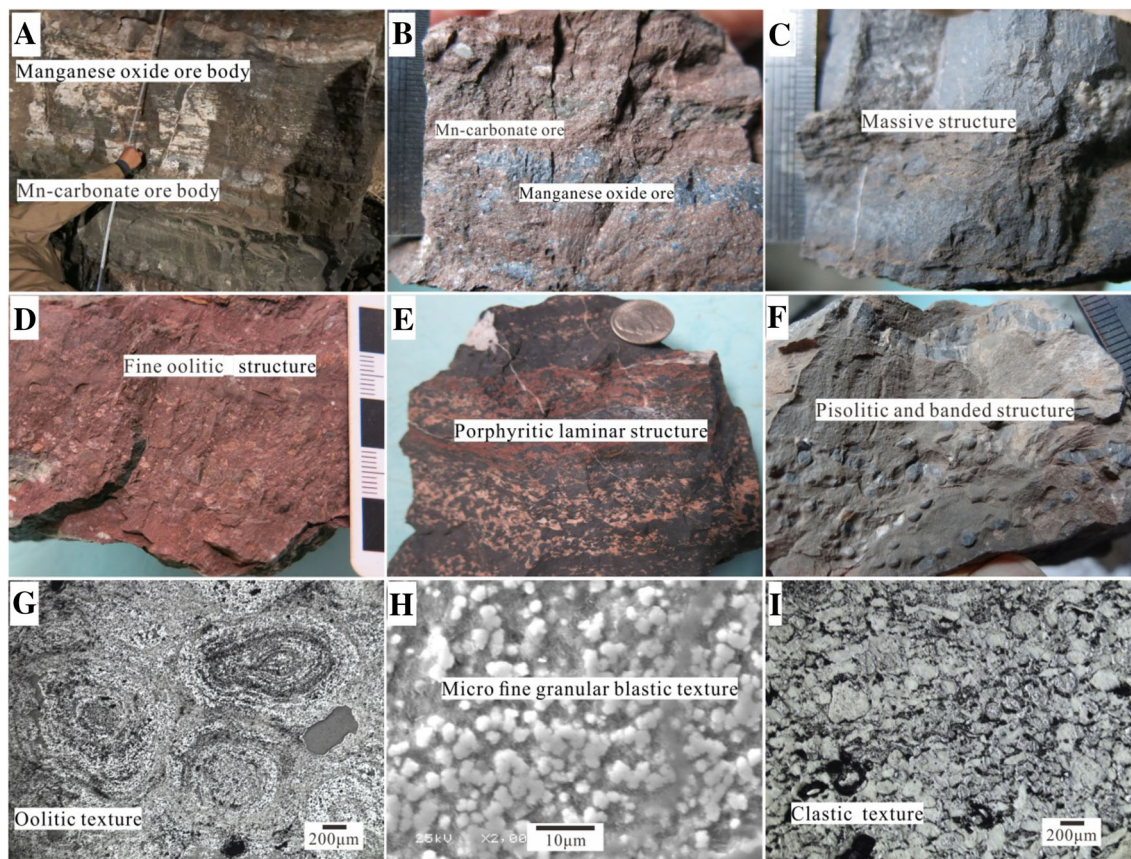
Fig. 4 Manganese-bearing rock series, morphology of ore bodies, and ore structures and textures of the Dounan manganese deposits in the southeastern Yunnan, China. **a** Manganese-bearing rock series in Baigu; **b** massive structure, manganese oxide ore and Mn-carbonate interbeded; **c** massive structure; **d** fine oolitic structure, manganese-carbonate ore; **e** porphyritic and laminar structure; **f** pisolitic and banded structure; **g** oolitic texture; **h** micro fine granular blastic texture; **i** clastic texture

collected from the V_1 ore bed in the Gake section, including 7 ore samples and 3 top and bottom plates and interlayer samples. Eleven samples were collected from the V_7 and V_8 ore beds in the Baigu section, with 6 ore samples and 5 top and bottom plates and interlayer samples. Major-, trace-, and rare-earth element analysis tests were performed on all samples (Tables 2, 3). Four representative samples were selected from the two ore sections for x-ray diffraction (XRD) mineralogy analysis and eight samples with higher Fe content were analyzed using ^{57}Fe Mössbauer spectroscopy. The sampling situation is shown in Table 1.

The samples were prepared as polished thin sections for petrographic study under transmitted polarizing and reflected light microscopes. The mineralogical analysis was conducted using XRD using a Philips X'Pert diffractometer. The bulk mineralogy was determined using semi-quantitative ($\pm$ 5%) XRD. The diffraction analyses were conducted in the State Key Laboratory of Ore Deposit Geochemistry, Guiyang Institute of Geochemistry, Chinese Academy of Sciences (SKLODG, GIGCAS, hereafter).

Mössbauer spectroscopy (MS) was performed at the Lanzhou Center for Oil and Gas Resources, Institute of Geology and Geophysics, Chinese Academy of Sciences. The samples were loaded in an acrylic holder with a relative thickness of 15 mg Fe per cm^2, and then irradiated with γ-rays from a 25 mCi ^{57}Co(Rh) radioactive source to obtain a room temperature Mössbauer spectrum. The Mössbauer spectrometer was calibrated using α-Fe as the reference and the product species were identified on the basis of their quadrupole and isomer shifts as well as their hyperfine magnetic fields with reference to the values available in the literature (Stevens et al. 1998). Curve fitting of the obtained spectra was performed using Win-Noroms-for-Igor. The percentage of various Fe species was provided by the peak area.

All samples were crushed to a 200-mesh size for whole-rock geochemical analyses. The major and trace elements were analyzed at the SKLODG, GIGCAS. The major elements were analyzed using X-ray fluorescence (XRF) using a PANalytical AXIOS instrument (Malvern Panalytical B.V., the Netherlands) following the method documented by Hu (2009). The detection limit for all the major oxides was 0.01 wt%. The analysis errors were less than 3%. The trace elements were analyzed by inductively-coupled

Table 1 Description of sampling locations along the representative profiles of the Dounan manganese deposits

Samples	Ore bed	Sampling location (top to bottom)	Mineral association	Lithology and sedimentary structure	Mössbauer	XRD
BG-1	V8	Roof	–	Grayish–green silty mudstone with horizontal bedding		
BG-2	V8	0–0.1 m	Braunite and Mn carbonates	Purple–red compact massive and stratoid ores		
BG-3	V8	0.1–02 m	Mn-bearing interlayer	Gray–black Mn-bearing silty mudstone		
BG-4	V8	0.2–0.4 m	Mn-bearing interlayer	Gray–black Mn-bearing siltstone	√	√
BG-5	V8	0.4–0.5 m	Mn carbonates	Purple–red massive Mn-carbonates with clastics	√	
BG-6	V8	0.5–0.7 m	Braunite	Black compact massive braunite with few clastics		√
BG-7	V8	0.7–0.8	Braunite and Mn carbonates	Braunite and Mn-carbonates interbedded, with micronodules		
BG-8	V8	0.8–1.0 m	Braunite and Mn carbonates	Purple–red Mn-carbonates mixed with black braunite, stratoid	√	
BG-9	V7	Roof	–	Gray siltstone		
BG-10	V7	∼ 0.5 m	Braunite and Mn carbonates	Mn-carbonates mixed with braunite, with clastics, stratoid		
BG-11	V7	Floor	–	Gray siltstone with numerous clastics		
GK-9	V1	Roof	–	Gray siltstone		
GK-8	V1	0–0.1 m	Braunite and Mn carbonates	Braunite and Mn-carbonates interbedded	√	
GK-7	V1	0.1–0.2 m	Mn carbonates	Purple–red massive Mn-carbonates, with clastics and micronodules	√	
GK-6	V1	0.2–0.4 m	Braunite and Mn carbonates	Braunite and Mn-carbonates interbedded		√
GK-5	V1	0.4–0.6 m	interlayer	Gray mudstone with horizontal bedding		
GK-4	V1	0.6–0.7 m	Braunite and Mn carbonates	Braunite transitional contact with Mn-carbonates	√	
GK-3	V1	0.7–0.9 m	Braunite	Black compact massive braunite interbedded with calcite		
GK-2	V1	0.9–1.1 m	Braunite and manganite	Black massive braunite and nodular manganite, with clastics		√
GK-1	V1	1.1–1.3 m	Braunite	Black stratoid braunite, with clastics and micronodules	√	
GK-0	V1	Floor	–	Gray bedded silty mudstone	√	

plasma-mass spectrometry (ICP-MS) using an ELAN-DRC-e instrument (PerkinElmer, USA) following the method documented by Qi et al. (2000). The detection limits were as follows: Tb, Ho, Lu, Cs, and Tm—0.01 ppm; Er, Eu, Sm, Pr, and Yb—0.03 ppm; Ba, Ce, Co, Th, Gd, Dy, and U—0.05 ppm; Ta, Nd, Ga, and Sr—0.1 ppm; Rb, Cu, Ni, Nb, and Hf—0.2 ppm; Y, Pb, and La—0.5 ppm; W and Sn—1 ppm; Zr and Mo—2 ppm; V—5 ppm; and Cr—10 ppm. The analysis errors were less than 10%.

5 Results

5.1 Petrology and mineralogy

Via hand specimens, microscopy, and XRD analysis of various ores (Table 2), manganese ores in the Dounan manganese deposit can be divided into three types of ore phases according to the characteristics of mineral combination and structural features as follows:

(1) *Mn oxide ore phase* the ores show compact massive, oolitic and pisolitic, and banded structures. The main manganese minerals are all brown manganese (Fig. 4c, f). The oolitic and pisolitic ore shapes are

Table 2 XRD analysis of manganese ore samples (%)

Samples/minerals	BG-4	BG-6	GK-2	GK-6
Braunite	√	√	√	√
Manganite	–	–	√	–
Ca-rhodochrosite	–	–	–	√
Kutnahorite	–	–	–	√
Mn-calcite	–	–	–	√
Quartz	√	–	√	–
Feldspar	√	√	√	√
Calcite	–	√	√	√
Dolomite	–	√	–	–
Clay minerals	√	√	–	√

"√" indicates that the sample contains the mineral in the qualitative analysis of XRD. "–" indicates that the mineral was not found

mostly spherical, ellipsoidal, or irregular, with a diameter of approximately 0.1–1.0 mm. Most have bright and dark concentric rings (Fig. 4g). The brightly-colored rings are mainly composed of braunite and a small amount of manganite (Fig. 5a, b), and the dark-colored rings consist of manganese carbonate minerals such as Ca-rhodochrosite and calcimangite (Fig. 5c). The banded ores are compacted from dense oolitic and pisolitic braunite, often forming a stratified structure in combination

with the dark and light interbedded layers of gray-green and purple-red manganese carbonates or other debris (Fig. 4e, f).

(2) *Mn carbonate ore phase* the ore is gray and purple-red and mostly has an oolitic and pisolitic structure (Fig. 4d). The diameter of the oolite is approximately 0.02–1.7 mm, and the interior has an unclear ring structure. The external shape is irregular. The manganese minerals are mainly Ca-rhodochrosite, calcimangite, Mn-bearing calcite, and kutnahorite (Fig. 5c).

(3) *Mixed ore phase (transitional ores)* the ore is a mixed purple and gray-brown. The ore minerals are characterized by the intermixing of manganese carbonates and braunite (Fig. 5d). Braunite often forms dark patches in the manganese carbonates (Fig. 4b, e). The ores show indistinct stratification because of later compaction (Fig. 4e). The gangue minerals are quartz, calcite, and dolomite.

5.2 Characterization of iron species

The ^{57}Fe Mössbauer spectra of the representative samples at room temperature (about 290 K) are shown in Fig. 6, in which three overlapping doublets and one sextet are observed. The Mössbauer parameters and relative abundance of the three different Fe species for the samples are

Table 3 Mössbauer parameters of Fe-components in the bulk samples of the Dounan Manganese deposit

Samples	Iron species	Components	Relative content %	IS/mm s^{-1}	QS/mm s^{-1}	HW/mm s^{-1}	Hi/T
BG-4	para-Fe^{2+}	Kaolinite	59.8	1.14 ± 0.00	2.69 ± 0.01	0.19 ± 0.01	
	para-Fe^{3+}	Chlorite	40.2	0.38 ± 0.01	0.83 ± 0.03	0.31 ± 0.02	
BG-5	hem-Fe^{3+}	Hematite	91.6	0.38 ± 0.01	− 0.21 ± 0.01	0.16 ± 0.01	51.28 ± 0.02
	para-Fe^{3+}	Kaolinite	8.4	0.35 ± 0.07	0.66 ± 0.10	0.31 ± 0.08	
BG-8	hem-Fe^{3+}	Hematite	54.8	0.39 ± 0.01	− 0.21 ± 0.02	0.18 ± 0.02	51.11 ± 0.07
	para-Fe^{3+}	Kaolinite	30.1	0.35 ± 0.04	0.67 ± 0.08	0.30 ± 0.02	
	para-Fe^{2+}	Kaolinite	14.1	1.18 ± 0.09	2.61 ± 0.18	0.19 ± 0.04	
GK-8	para-Fe^{3+}	Kaolinite	42.8	0.44 ± 0.05	0.73 ± 0.09	0.48 ± 0.20	
	para-Fe^{2+}	Kaolinite	57.2	1.12 ± 0.01	2.64 ± 0.02	0.16 ± 0.03	
GK-7	hem-Fe^{3+}	Hematite	77.3	0.38 ± 0.01	− 0.21 ± 0.01	0.28 ± 0.02	51.27 ± 0.05
	para-Fe^{3+}	Illite	12.2	0.34 ± 0.09	0.82 ± 0.18	0.27 ± 0.09	
	para-Fe^{2+}	Kaolinite	10.5	1.16 ± 0.09	2.58 ± 0.18	0.25 ± 0.10	
GK-4	hem-Fe^{3+}	Hematite	86.4	0.38 ± 0.00	− 0.19 ± 0.00	0.16 ± 0.01	51.35 ± 0.01
	para-Fe^{3+}	Illite	13.6	0.30 ± 0.00	0.82 ± 0.03	0.39 ± 0.08	
GK-1	hem-Fe^{3+}	Hematite	100	0.39 ± 0.01	− 0.20 ± 0.01	0.15 ± 0.02	51.49 ± 0.04
GK-0	hem-Fe^{3+}	Hematite	61.3	0.37 ± 0.01	− 0.19 ± 0.01	0.16 ± 0.02	51.56 ± 0.03
	para-Fe^{3+}	Kaolinite	14.5	0.41 ± 0.02	0.75 ± 0.03	0.37 ± 0.03	
	para-Fe^{2+}	Kaolinite	24.2	1.13 ± 0.00	2.65 ± 0.01	0.19 ± 0.02	

IS isomer shifts, *QS* quadruple splitting, *HW* half width at half maximum, *Hi* hyperfine field
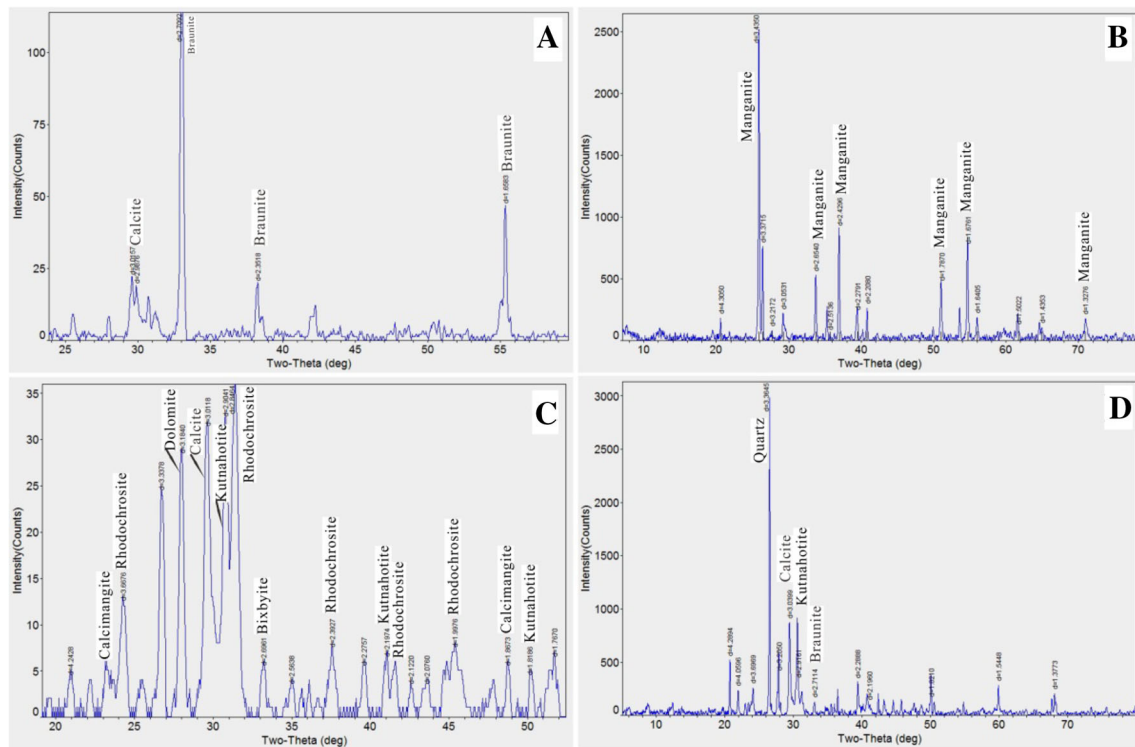
Fig. 5 X-ray diffractograms of **a** braunite, **b** manganite, **c** manganese carbonate minerals, **d** paragenesis of kutnahotite and braunite and some gangue minerals
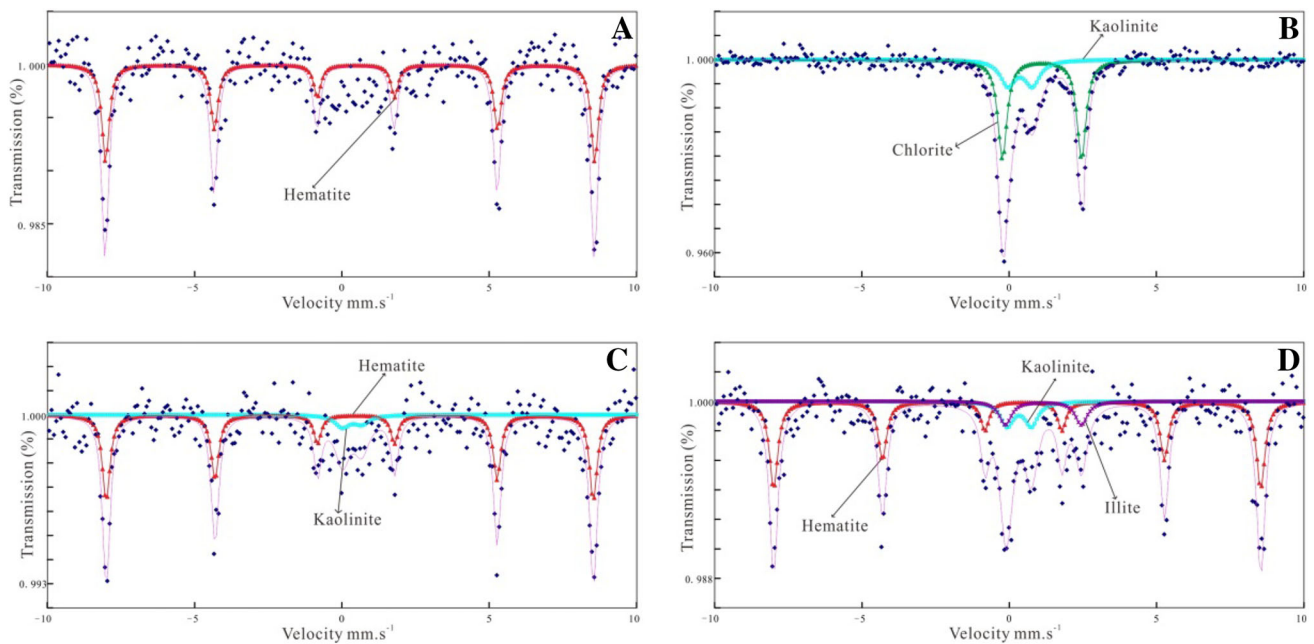

Fig. 6 Mössbauer spectrum of the bulk samples in the Dounan manganese deposit. **a** Hematite; **b** kaolinite (Fe^{2+}) and chlorite (Fe^{3+}); **c** α-hematite (Fe^{3+}) and kaolinite (Fe^{3+}); **d** hematite (Fe^{3+}), illite (Fe^{3+}) and kaolinite (Fe^{2+})

summarized in Table 3. The doublet with a smaller quadrupole splitting was ascribed to paramagnetic high-spin Fe^{3+} (*para*-Fe^{3+}) (Manning and Ash 1979), and according to the isomer shift of 0.30–0.38 and quadrupole splitting of 0.66–0.83, the components originated from clay minerals such as kaolinite, chlorite and illite with Fe^{3+}. The doublet with the larger isomer shift (1.12–1.18) and quadrupole splitting (2.58–2.69) was attributed to paramagnetic high-

spin Fe^{2+} (*para*-Fe^{2+}) comprising kaolinite with Fe^{2+}. The sextet with an isomer shift of 0.37–0.39, quadrupole splitting of -0.21 to -0.19, and hyperfine field of 51.11–51.56 T was designated antiferromagnetic hematite (α-Fe_2O_3, *hem*-Fe^{3+}). The curve fitting for these four components is reliable because the Chi squared values are sufficiently small. According to the relative content relationship, Fe^{3+} is the main valence state of iron. The minerals of most of the ore beds are mainly hematite (α-Fe_2O_3) and a small amount of ferric clay minerals, and a few contain only Fe^{3+} clay minerals, such as BG-4 and GK-8. Fe^{2+} is present in the clay minerals (kaolinite Fe^{2+}). Pyrite or other ferruginous minerals were not found in the tested samples.

5.3 Geochemistry

The major elements of the 21 samples are shown in Table 4. The Mn content of the manganese ore sample in the Baigu section is from 8.71 to 52.2% (mean 24.1%), and the Mn content in the Gake ore sample is from 14.6 to 48.1% (mean 39.3%). The Mn/Fe ratios range from 3.53 to 169 (mean 49.5) and from 5.12 to 160 (mean 56.4), respectively. The Mn content of all the top and bottom plates and interlayers is from 0.63 to 5.24%. The P and S of all samples were less than 1%, Overall, the ore was characterized by high Mn, low Fe, and minimal P and S. The loss on ignition (LOI) ranged from 4.67 to 35.6% (average 17.6%), indicating that the manganese ore contained a certain number of carbonate and water-containing components. The manganese ore layer is relatively depleted of Si, Al, Ti, and K compared to the top and bottom plates and interlayers.

The occurrence state of trace elements and their degree of enrichment in the sediments are useful for indicating the sedimentary environment (Tribovillard et al. 2006). Therefore, the environment can be reconstructed by the content or ratio of trace elements in sediment, such as V/Cr, V/(V + Ni), Sr/Ba, etc. However, there are great differences in the sources of trace elements in sediments, and some may have multiple sources. Thus, when reconstructing sedimentary environments, trace elements that are mainly authigenic and have retained their initial content should be selected to accurately indicate the environmental conditions during deposition. Generally, if some trace elements are suspected to be of mixed origin, that is, detrital and authigenic, the authigenic fraction can be estimated as the part in excess of the average shale abundance. The clastic fraction of element X in a sample can be estimated as follows: detrital X = (X/

Table 4 Major elements compositions (wt%) of the Dounan manganese deposit

	Al_2O_3	CaO	FeO	K_2O	MgO	MnO	Na_2O	P_2O_5	SiO_2	SO_3	TiO_2	LOI	Total	Mn/Fe
BG-1	13.9	4.29	4.73	3.30	3.29	0.81	1.35	0.14	57.5	0.11	0.67	8.04	98.2	0.17
BG-2	1.90	21.6	4.38	0.29	2.10	27.1	0.47	0.17	9.79	0.05	0.08	28.5	96.3	6.15
BG-3	11.1	6.45	2.48	2.56	2.84	6.25	1.31	0.15	52.3	0.04	0.56	12.1	98.2	2.52
BG-4	13.3	4.12	3.01	2.87	3.08	1.19	1.78	0.13	60.8	0.24	0.65	7.21	98.4	0.39
BG-5	1.53	34.8	2.36	0.29	4.12	11.7	0.28	0.14	6.73	0.20	0.07	35.6	97.8	4.95
BG-6	1.04	5.72	0.40	0.03	1.32	67.4	0.10	0.14	10.21	0.02	0.04	7.50	93.9	169
BG-7	1.28	10.3	0.51	0.08	2.14	55.2	0.18	0.17	11.2	0.03	0.06	13.6	94.7	107
BG-8	5.79	18.7	2.16	1.41	4.76	14.3	0.56	0.16	23.8	0.33	0.26	26.2	98.5	6.58
BG-9	12.7	6.90	2.91	3.05	2.46	2.63	1.30	0.13	56.3	0.20	0.61	10.1	99.3	0.90
BG-10	5.91	20.3	3.17	0.99	2.62	11.2	1.60	0.10	27.1	0.04	0.27	24.6	97.9	3.53
BG-11	11.5	8.09	3.78	2.57	2.25	0.82	1.01	0.15	57.1	2.37	0.61	9.87	100	0.22
GK-9	6.29	20.4	6.58	1.54	7.06	5.78	0.39	0.27	23.1	0.06	0.25	26.1	97.8	0.87
GK-8	4.42	18.6	1.57	1.06	3.80	21.7	0.25	0.15	17.04	0.14	0.20	29.6	98.4	13.8
GK-7	4.51	19.8	3.06	1.08	4.15	18.8	0.21	0.25	17.4	0.10	0.21	28.8	98.3	6.12
GK-6	1.78	10.5	0.58	0.03	1.85	54.2	0.31	0.19	11.0	0.04	0.06	14.5	95.0	93.6
GK-5	16.3	0.61	3.91	3.61	4.01	1.17	1.95	0.15	61.7	0.02	0.73	4.67	98.9	0.30
GK-4	8.56	11.2	8.98	1.41	6.76	6.76	1.26	0.29	35.8	0.04	0.46	16.5	98.0	0.75
GK-3	1.34	11.3	0.38	0.01	1.22	60.9	0.08	0.13	9.18	0.15	0.04	9.48	94.1	160
GK-2	1.58	10.6	0.55	0.01	1.39	62.1	0.05	0.13	8.85	0.19	0.06	9.74	95.2	112
GK-1	3.10	20.8	4.37	0.52	7.30	22.5	0.37	0.21	11.0	0.07	0.14	26.5	96.9	5.12
GK-0	14.5	2.59	5.03	3.24	3.93	4.74	1.39	0.19	54.8	0.08	0.65	6.98	98.1	0.94

Al)$_{average\ shale}$ × Al$_{sample}$ (average shale = Wedepohl 1971, 1991). Consequently, the authigenic fraction of element X is calculated as total X – detrital X (Tribovillard et al. 2006).

According to this calculation (Table 5), Ba in the ore beds of Baigu is mainly from detrital components, while the Ba in the ore beds of Gake is mainly from authigenic components. The content of authigenic Sr in all the samples of Baigu and Gake is significantly higher than that of the tops, bottoms, and interlayers (Fig. 7a). Apart from the individual rock and ore layers, the proportions of the authigenic components of Ni and V are relatively higher (Fig. 7c, d), and the relative contents of the Baigu and Gake ore sections are similar. Cr in the authigenic components in Baigu and Gake is significantly lower (Fig. 7b), indicating that most of the Cr were provided by detrital materials. Therefore, V/Cr and Sr/Ba are not suitable to indicate the sedimentary environment of the Dounan manganese deposit, but V/(V + Ni)$_{auth}$ is a credible redox proxy with minimal detrital influence. As shown in Fig. 9a, after deducting the detrital part, the V/(V + Ni)$_{auth}$ ratios of the samples in Baigu ranged from 0.22 to 0.75 (mean 0.41), which vary greatly in the vertical profiles and show an "S" type spread (BG-8 in excessive debris was not taken into account). The V/(V + Ni)$_{auth}$ ratios of the samples in Gake ranged from 0.03 to 0.87 (mean 0.38), and the ratios of the manganese ore layer were small and relatively concentrated, while the ratios in the top and bottom plates and interlayers were larger. The Sr content of the authigenic components of the Baigu and Gake is similar in most of the ore beds, but they have different characteristics in the profile (the BG-9 in excessive debris was not taken into account). The Sr content of Baigu varies greatly, but relatively concentrated in Gake (Fig. 9b).

The Post Archean Australian Shale (PAAS)-normalized rare-earth-element (REE) patterns are similar among the Baigu and Gake ore blocks and wall rocks (Fig. 8a, b). The $\sum$REE contents of the Baigu and Gake samples show obvious changes in the vertical profiles (Fig. 9c). The δCe of Baigu ranged from 0.79 to 97 (mean 0.91) (δCe = 2(Ce/Ce$_N$)/(La/La$_N$ +Pr/Pr$_N$), "N" stand for PAAS. The overall performance showed a weak negative anomaly (Fig. 8a). The δCe values of Gake ranged from 0.74 to 1.23 (mean 1.01). Figure 8b shows that there are differences in the δCe characteristics of Gake and Baigu. Figure 9d shows that the δCe values of the two ore sections are all close to 1, and the variation range is small; however, there are some changes among the mineral layers.

6 Discussion

The study of the Sedimentary environment is an important part of the study of the mineralization mechanism of manganese deposits. Different sedimentary environments have obvious effects on the migration, enrichment, and precipitation of manganese, as well as the types of manganese minerals present and the morphology of ore bodies. The depositional environment of Dounan has long been a subject of speculation and discussion. Previous researchers studied the Dounan manganese deposit from an overall perspective, but there are many differences between the ore-forming environments of different ore beds. Additionally, the impact of environmental change on the profile of the different ore beds is not fully understood. Therefore, specific environmental factors, such as Eh, pH, ore-forming depth, salinity, etc. remain worth exploring.

As previously mentioned, the Dounan manganese deposit is in the Dounan basin on the western edge of the Yangtze platform in South China. The basin is in a semi-confined gulf environment surrounded by paleocontinents on three sides (Fig. 1), which could receive the weathered and eroded materials containing manganese from the paleocontinents and limit the materials exchange between the basin and the outer Tethys Ocean. The lithology of the ore-bearing layer is a set of mudstone, siltstone, and sandstone, interbedded with carbonate, and the sedimentary structure is dominated by horizontal bedding and low-angle cross-bedding (Liu et al. 1984), suggesting that the depositional conditions were mainly shallow marine with relatively agitated water. The mineral compositions of each ore bed are braunite, manganite, Ca-rhodochrosite, calcimangite, etc., and there are nearly no primary manganese oxides with Mn^{4+}. According to studies of the chemical conditions of precipitation of various manganese minerals by Krauskopf (1957) and Roy (2006), braunite and Mn-carbonates form and deposit under weakly oxidizing alkaline conditions and weakly reducing alkaline conditions, respectively. Therefore, the depositional environment of the Dounan manganese deposit was a weak oxidation-weak reduction environment. In the near-shore shallow marine environment, abundant biodegradation of algal microbes releases H_2S, CO_2, and other gases into the metallogenic environment. The small amount of H_2S dissipates quickly in shallow water, and the CO_2 dissolves in the water, creating an aqueous medium that is weakly alkaline, which is favorable for the accumulation and deposition of Mn. In the vertical profiles, the two main ore sections of Baigu and Gake exhibit the characteristics of a manganese oxide ore phase, manganese carbonate ore phase, and mixed ore phase gradually changing or mutating, indicating that the redox conditions during different

Table 5 Trace elements and REEs compositions (ppm) of the Dounan manganese deposit

	BG-1	BG-2	BG-3	BG-4	BG-5	BG8-6	BG-7	BG-8	BG-9	BG-10	BG-11	GK-9	GK-8	GK-7	GK-6	GK-5	GK-4	GK-3	GK-2	GK-1	GK-0
V	585	47.0	163	445	110	69.0	44.0	37.0	282	83.0	158	56.0	299	45.6	53.9	729	71.3	131	127	68.4	953
Cr	90.0	10.0	70.0	100	20.0	10.0	10.0	50.0	70.0	30.0	80.0	40.0	38.7	27.6	12.8	103	84.1	10.4	12.1	27.5	106
Co	38.0	13.0	30.0	63.0	17.0	87.0	58.0	31.0	25.0	37.0	41.0	31.0	53.9	35.5	25.2	111	93.0	88.9	94.5	38.1	191
Ni	212	103	99.0	200	50.0	206	187	121	263	154	116	99.0	70.3	82.5	142	160	199	285	235	193	287
Cu	11.0	9.00	32.0	76.0	3.00	54.0	41.0	9.00	14.0	9.00	50.0	6.00	43.2	6.42	18.2	61.7	27.6	37.2	38.4	32.9	79.4
Zn	119	37.0	100	112	24.0	71.0	61.0	55.0	127	66.0	85.0	57.0	62.9	54.9	67.5	169	108	65.6	69.3	59.3	145
Rb	155	14.4	123	142	14.0	1.80	4.30	67.3	139	47.3	122	74.8	48.3	49.8	2.95	175	69.4	0.37	0.84	26.4	144
Sr	358	1040	357	264	771	130	297	477	186	307	302	417	420	393	372	303	355	317	321	463	403
Y	24.5	14.1	24.4	25.3	12.6	6.00	8.10	18.8	20.5	16.5	25.6	29.5	15.1	16.3	11.4	23.1	30.6	8.81	9.64	24.8	27.1
Zr	160	32.0	140	173	26.0	13.0	19.0	83.0	145	108	172	66.0	44.8	49.2	17.8	153	127	14.7	18.0	40.9	152
Nb	11.4	1.70	9.90	11.5	1.80	0.80	1.20	5.00	9.70	5.00	10.4	5.30	3.80	4.30	1.37	12.9	8.96	1.43	1.68	3.96	12.8
Cs	9.98	0.64	7.54	8.55	0.77	0.08	0.17	3.47	8.53	2.74	7.87	4.22	3.30	3.29	0.29	13.4	5.57	0.05	0.07	1.68	9.75
Ba	326	148	243	270	78.4	26.8	84.0	154	242	122	223	192	154	192	70.9	556	337	2590	3280	219	434
Pb	4.00	31.0	11.0	9.00	11.0	72.0	58.0	23.0	17.0	33.0	20.0	24.0	9.70	6.42	9.51	14.1	29.6	12.7	13.9	22.2	26.0
Th	13.0	1.93	11.0	12.7	1.74	0.85	1.33	5.28	11.2	6.91	11.3	5.05	4.39	4.68	1.56	16.1	9.81	0.89	1.19	3.15	12.0
U	3.42	0.72	2.63	9.56	1.83	3.67	2.65	2.00	3.21	1.61	5.49	1.27	4.45	1.57	1.24	7.33	2.02	3.25	2.71	2.10	10.0
La	33.6	8.80	30.1	32.8	9.60	4.20	6.60	18.8	26.6	14.6	31.3	25.6	15.2	16.3	8.86	26.0	30.0	8.36	8.42	22.0	29.0
Ce	63.4	17.4	57.7	63.4	17.9	6.30	10.3	39.5	48.2	30.2	62.1	63.5	35.0	37.7	13.0	52.2	60.4	12.1	14.6	53.7	66.0
Pr	7.28	2.31	6.55	7.17	1.90	0.80	1.29	4.66	5.63	3.99	7.01	6.33	3.34	3.56	1.83	5.94	6.69	1.57	1.56	4.63	7.13
Nd	23.0	8.70	21.8	23.2	7.00	3.00	4.80	15.8	19.0	14.7	23.2	22.2	12.9	14.2	7.31	21.8	27.1	6.05	6.58	18.5	27.0
Sm	4.48	2.04	4.54	4.66	1.66	0.69	1.12	3.30	3.78	3.17	4.67	4.65	3.02	2.91	1.51	4.79	5.96	1.23	1.26	3.77	5.37
Eu	1.00	0.53	0.99	1.01	0.42	0.20	0.24	0.82	0.92	0.79	1.08	1.44	0.59	0.66	0.33	0.80	1.26	0.27	0.35	1.00	1.12
Gd	3.99	2.13	4.20	4.16	1.70	0.77	0.99	2.97	3.55	2.97	4.47	4.84	2.85	2.80	1.70	4.68	5.99	1.28	1.56	4.21	4.84
Tb	0.68	0.35	0.68	0.70	0.29	0.13	0.19	0.50	0.59	0.51	0.75	0.79	0.49	0.48	0.30	0.73	1.02	0.24	0.20	0.69	0.82
Dy	3.68	1.81	3.95	3.98	1.56	0.71	1.01	2.93	3.28	2.80	4.11	4.21	2.63	2.96	1.62	4.34	5.88	1.29	1.27	4.15	4.82
Ho	0.89	0.43	0.87	0.90	0.37	0.16	0.24	0.61	0.75	0.65	0.91	0.94	0.58	0.58	0.35	0.96	1.27	0.28	0.27	0.84	0.94
Er	2.48	0.98	2.47	2.53	1.00	0.43	0.64	1.75	2.08	1.63	2.51	2.58	1.44	1.71	1.05	3.35	3.56	0.92	0.83	2.16	3.12
Tm	0.42	0.17	0.39	0.44	0.14	0.07	0.11	0.27	0.38	0.28	0.40	0.41	0.20	0.25	0.17	0.48	0.59	0.12	0.12	0.33	0.48
Yb	2.53	0.78	2.41	2.53	0.81	0.44	0.57	1.49	2.20	1.57	2.43	2.38	1.16	1.40	0.87	3.23	3.19	0.65	0.64	1.94	2.82
Lu	0.40	0.14	0.36	0.40	0.14	0.06	0.08	0.24	0.34	0.25	0.39	0.40	0.20	0.24	0.16	0.50	0.50	0.12	0.11	0.27	0.43
ΣREE	147	46.6	137	148	44.5	18.0	28.2	93.6	117	78.1	145	140	79.6	85.8	39.1	129	153	34.5	37.8	118	155
δCe	0.94	0.89	0.95	0.95	0.97	0.79	0.81	0.97	0.91	0.91	0.97	1.15	1.13	1.14	0.74	0.97	0.98	0.77	0.93	1.23	1.06
V/(V + Ni)$_{auth}$	0.75	0.25	0.59	0.70	0.69	0.23	0.16	–	0.46	0.22	0.50	0.09	0.83	0.14	0.23	0.87	0.03	0.30	0.33	0.20	0.79
Cr$_{auth}$	15.3	–	10.3	28.6	11.8	4.43	3.14	19.0	2.10	–	18.7	6.29	15.0	3.43	3.26	15.5	38.2	3.22	3.63	10.9	28.2
Ni$_{auth}$	155	95.3	53.9	146	43.8	201	181	97.6	212	130	69.4	73.5	52.4	64.2	134	93.9	164	279	229	180	228
V$_{auth}$	477	32.3	76.8	341	98.2	61.0	34.1	–	184	37.3	68.8	7.31	265	10.7	40.1	602	120	5.04	115	44.4	840

Table 5 continued

	BG-1	BG-2	BG-3	BG-4	BG-5	BG8-6	BG-7	BG-8	BG-9	BG-10	BG-11	GK-9	GK-8	GK-7	GK-6	GK-5	GK-4	GK-3	GK-2	GK-1	GK-0
Ba_{auth}	–	82.9	–	–	25.6	–	39.8	–	–	–	–	–	1.34	36.2	9.42	–	41.4	2543	3225	111	–
Sr_{auth}	109	1006	158	25.9	743	111	274	373	–	201	96.2	304	341	312	340	11.5	202	293	293	407	143

stages of the ore-forming process changed, and the ore-forming location was probably near the redox interface.

Geochemically, a suite of trace elements can exhibit somewhat different sensitivities to the sedimentary environment (Tribovillard et al. 2006). The corresponding redox classification of sedimentary environments includes oxic, suboxic, anoxic, and euxinic facies, which estimate the oxygen tensions associated with these environments: > 2.0, 2.0–0.2, < 0.2 and 0 ml O_2 L^{-1} H_2O, respectively (Edwards 1985; Tyson and Pearson 1991). In the case of mainly authigenic components, the V/(V + Ni)$_{auth}$ value can reflect the redox environment during the formation of sediments. A value of V/(V + Ni)$_{auth}$ ranging from 0 to 0.46 represents an oxidizing environment, 0.46–0.57 a weakly oxidizing environment, 0.57–0.83 a weakly reducing environment, and 0.83–1 a reducing environment (Jones and Marning 1994; Wignall 1994). The V/(V + Ni)$_{auth}$ ratios of the samples in Baigu is from 0.22–0.75, and the characteristics of the profiles are shown in Fig. 9a. Five samples fall within a range of 0–0.46, one sample 0.46–0.57, and four samples 0.57–0.83, indicating that the redox conditions of the different layers vary among oxidation, weak oxidation, and weak reduction conditions, respectively. The V/(V + Ni)$_{auth}$ ratios of Gake range from 0.03 to 0.87. Except for the bottom plate GK-0, the interlayer GK-5, and the ore layer GK-8, the other samples all fall within the range of from 0 to 0.46, indicating that the metallogenic environment was dominated by oxidation, and the change trend is relatively stable. The characteristics of $\sum$REE content in the profiles of Baigu and Gake are shown in Fig. 9c. There are obvious changes in $\sum$REE content between the two ore sections, suggesting that the environment changed during the ore-forming process. The δCe values of the two ore sections are all close to 1 (Fig. 9d). The REE patterns normalized by PAAS (Fig. 8a, b) show that Ce is between weak positive anomalies and weak negative anomalies, showing changes between weak oxidation and weak reduction in the ore-forming environment. Both δCe and V/(V + Ni) reflect the changes in the redox conditions of the ore-forming environment in the different layers of the Baigu and Gake, but the results of the two are not completely consistent. This is because in addition to the possible effects of debris, in a suboxic environment, Ce-containing sediments are mobilized such that Ce is released into the water column resulting in a lower negative anomaly in the sediments (DeBaar 1991; Sholkovitz and Schneider 1991). In general, the δCe of a ridge expansion center is ∼ 0.29, an ocean basin ∼ 0.55, and a continental margin ∼ 0.9–1.3 (Murray et al. 1990). The δCe of the Baigu and Gake ore sections in the Dounan manganese deposit ranged from 0.74 to 1.23 (mean 0.96), indicating that the sedimentary
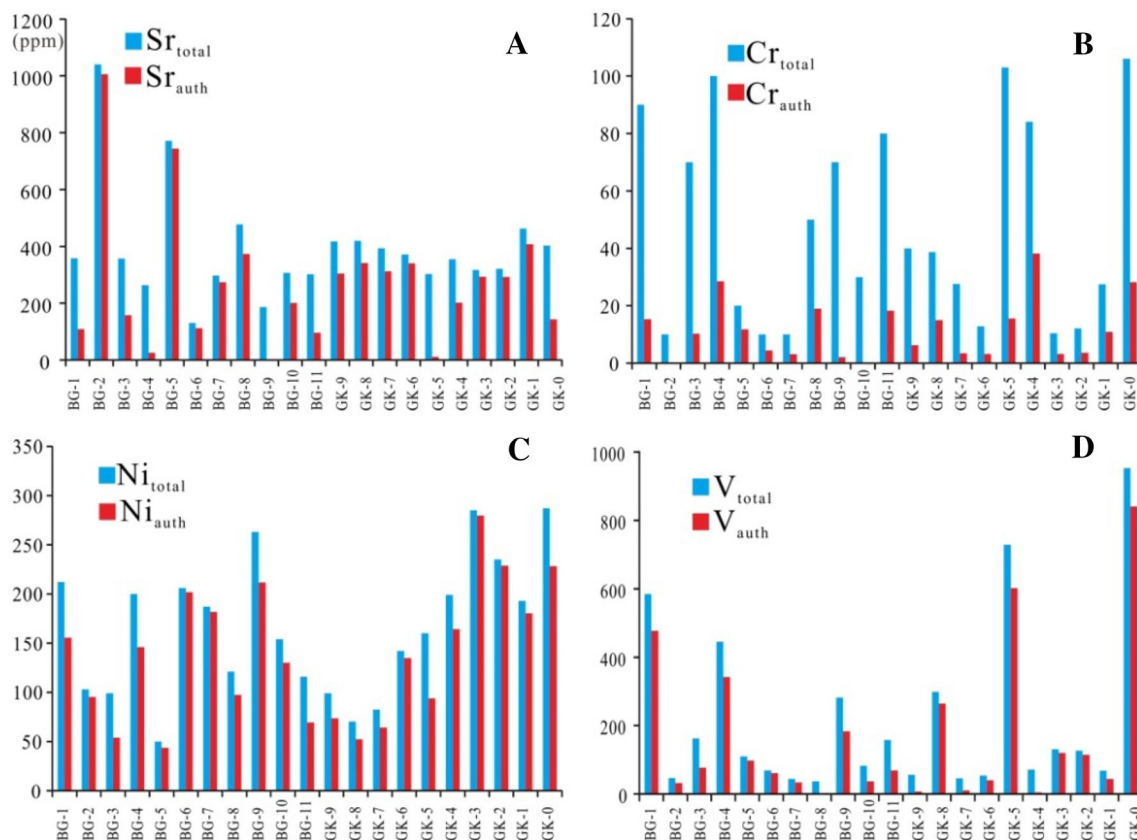
Fig. 7 Concentrations (ppm) of total and authigenic portions of elements Sr, Cr, Ni, and V of the samples in the Dounan manganese deposit
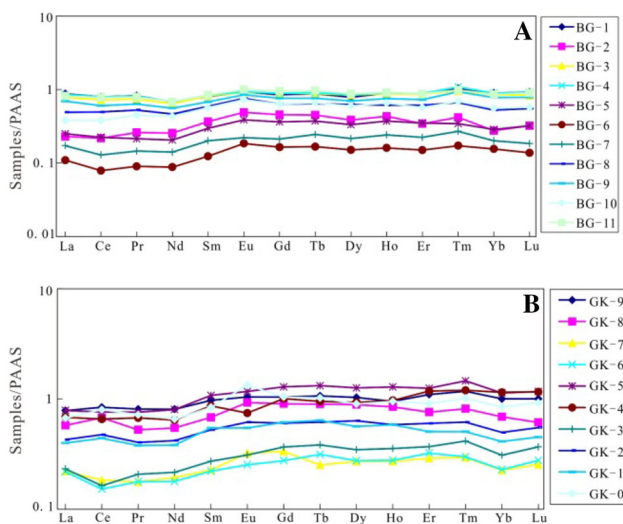

Fig. 8 PAAS-normalized REE patterns for bulk samples of the Dounan manganese deposit

environment during the ore-forming process was compatible with the continental margin environment. This result is consistent with that of the paleogeographic analysis. The Sr content is closely related to seawater salinity and shows a positive correlation (Klein et al. 1996). The majority of Sr in the Baigu and Gake are derived from authigenic

components (Fig. 7a), and the Sr content in the authigenic components ranged from 96.2 to 743 ppm and 143 to 407 ppm, respectively, both of which reflect a normal salinity environment. The abnormal Sr may have been caused by the high content of carbonate minerals. However, the characteristics of Sr variation in the vertical profiles of the two ore sections are different. The Sr content in the Baigu has a significant change from layer to layer, while the Sr content in the Gake tends to be relatively stable (Fig. 9b), indicating the former's metallogenic environment changed more frequently. Many biological features such as *lamellibranchs*, *gastropods*, and bacteria and algae were found in the ore section (Liu et al. 1984), and no gypsum minerals that could have formed in an arid climate have been found, indicating that the Dounan manganese deposit formed in warm weather conditions under normal salinity along a continental margin in a shallow-marine environment (Su 1983).

The Mössbauer spectrum of different Fe species had proven to be useful in classifying paleosedimentary environments and determining redox conditions of sediments (Berner 1981; Zheng et al. 2001). According to the well-documented behavior of Fe in marine sediments, Fe^{3+} primarily forms amorphous ferric oxyhydroxides (Coey et al. 1974; Konhauser et al. 2005) which are converted via
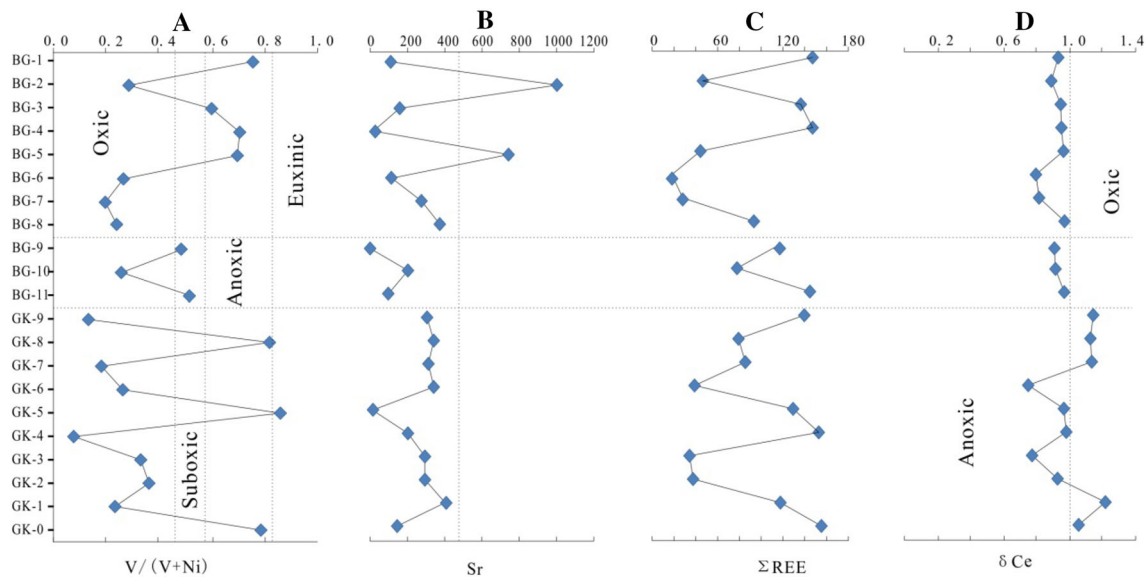
Fig. 9 The tendency chart of element ratios for the Dounan manganese deposit

dehydration and diagenesis to more stable minerals such as hematite (α-Fe_2O_3) (Ahn and Buseck 1990; Morris and Horwitz 1983; Sun et al. 2015). However, hematite dehydrated from ferric oxyhydroxide precursors during early

Fig. 10 Distribution profiles of various Fe species with ratios of Fe^{2+}/Fe^{3+} in the Dounan manganese deposit

diagenesis could have been further modified during subsequent diagenetic, hydrothermal, metamorphic, tectonic, or supergenetic processes. For example, oxyhydroxides could have transformed into acicular, fibrous, spindle-like, or microplaty hematite when occurring with oxidative meteoric fluids (Rasmussen et al. 2014). According to Mössbauer spectral data, the Fe^{3+} in the Dounan manganese deposit is mainly represented by hematite (α-Fe_2O_3), and there is no other ferric minerals except a small amount of clay minerals with Fe^{2+} and Fe^{3+}, indicating that the metallogenic environment was an ordinary sedimentary environment and there was no obvious hydrothermal activity during the mineralization process (Rasmussen et al. 2014; Sun and Li 2017). Normally para-Fe^{3+} in modern sediments is believed to be silicate Fe transported from the surroundings (Matsuo et al. 1996), while para-Fe^{2+} in sediments is supposed to exist in clay minerals as well as in amorphous Fe sulfide, carbonates, and/or in organically-bound forms (organic-Fe^{2+}) (Hilton et al. 1986; Matsuo et al. 1996). Comparing isomer shifts and quadrupole splitting values, para-Fe^{3+} and para-Fe^{2+} in the samples were confirmed to be clay minerals with less content, and there is no amorphous Fe sulfide or other forms of Fe^{2+} found in the Dounan manganese deposit. Some of the Fe^{3+} liberated from para-Fe^{3+} and hem-Fe^{3+} could have been diagenetically reduced and moved into clay minerals (Banwart 1999; Tuccillo et al. 1999), changing the pattern of para-Fe^{3+} and para-Fe^{2+}; thus, the distribution of para-Fe^{3+} and para-Fe^{2+} may indicate a change in the primary sedimentary conditions between the upper and lower ore beds. Figure 10 shows that the changing characteristics in the profile of para-Fe^{3+} and
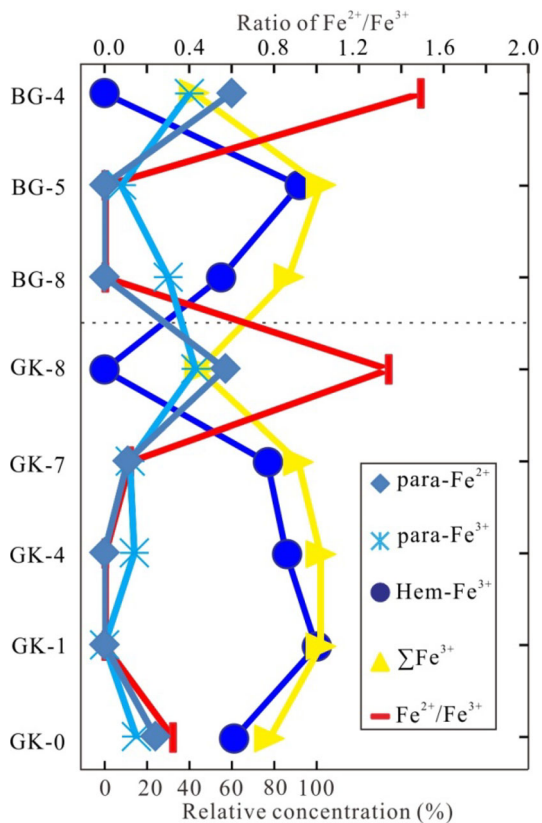
para-Fe^{2+} in the Baigu and Gake sections are similar, indicating that they share the same source, and that the diagenetic transformation caused by redox during the later period of mineralization was limited. The Fe^{2+}/Fe^{3+} (*hem*-Fe^{3+} + *para*-Fe^{3+}) ratio of modern and ancient sediments should be a good indicator for estimating sedimentary redox conditions (Kubo et al. 1996; Kuno et al. 1998). Except for BG-4 and GK-8, the Fe^{2+}/Fe^{3+} ratios of the other samples in the Baigu and Gake are all less than 1, indicating that the ore-forming environment was dominated by oxidation or sub-oxidation. Furthermore, the distribution characteristics of this value in the profiles show that the redox conditions during the ore-forming process vary from layer to layer (Fig. 10). The conclusion of Fe species analysis is consistent with the previous discussion. However, there is not complete agreement, such as the results of BG-5 and GK-0. Therefore, when geochemical indexes are used to study a metallogenic environment, it is necessary to fully consider the limitations of a single index and the contingency of the results obtained. Comprehensive utilization of multiple parameters is an effective method to obtain accurate results.

Summarizing the analysis of mineralogy, geochemistry, and Fe species strongly suggests that the Dounan manganese deposit formed in a shallow marine sedimentary basin on the continental margin with normal salinity. The physical and chemical conditions of ore formation were weakly alkaline and weakly oxidizing-weakly reducing. The ore-forming location was near the redox interface. The metallogenic environment of Gake in the lower ore section changed very little, except for individual ore layers and the top and bottom. The ore-bearing layer is mainly characterized by oxidation. The metallogenic environment of Baigu in the upper ore section shows fluctuations between weakly oxidizing and weakly reducing, showing that both the metallogenic depth and the redox interface fluctuated. This is consistent with the previous understanding of the incidents of transgression and regression events during the Middle Triassic (Anisian–Ladinian) in the southeastern Yunnan (Wu and Zhu 1994).

The characteristics of the redox conditions during the mineralization of the two major ore sections may reflect that the marine environment was at the beginning of transgression or the end of regression during the initial stage of mineralization. Therefore, the ores formed at the bottom of the deposit are manganese oxide ores dominated by braunite. With further development of transgression, rising sea level led to a gradual reduction in ore-forming water. During the transition from weak oxidation to weak reduction, a transitional manganese ore mixed with braunite and manganese carbonates formed. When the transgression reached its peak, a manganese carbonate ore phase mainly formed in the ore beds.

Therefore, it is likely that the lower ore section of Gake may have formed during the transition from the beginning of a transgression to its peak and the process of transgression was slow and continuous, such that the manganese ore formed at its lower layer was dominated by braunite, and there was a shift to a reducing manganese ore along the ore beds. The characteristics of the redox properties of Baigu in the upper part indicate that the changes in sea level during the ore-forming process were small but frequent, resulting in the formation of interbedded layers of manganese oxide ores and manganese carbonate ores.

7 Conclusion

Based on the mineralogy, geochemistry and Fe species evidence described above, the following regarding the metallogenetic environment of the Dounan manganese deposit may be concluded:

(1) The Dounan manganese deposit is a sedimentary manganese deposit formed in an environment of the epicontinental marine basin with normal salinity. Its ore-forming location was near the redox interface, and the redox property was the dominant factor in mineralization. The physical and chemical conditions of manganese mineralization were generally characterized as weakly alkaline and fluctuating between weakly oxidizing and weakly reducing.

(2) The variations in V/(V + Ni), δCe, and Fe^{2+}/Fe^{3+} from the Dounan manganese deposit possibly reflect redox change in a metallogenetic environment. The rise and fall of sea level was an important factor controlling the change in the mineralization environment. The Dounan manganese deposit was probably subjected to periodic transgressions and regressions during the mineralization stage.

References

Ahn JH, Buseck PR (1990) Hematite nanospheres of possible colloidal origin from a Precambrian banded iron formation. Science 250:111–113

Bai WL, Wang XC, Du FY, Yang ZG (2010) The tectonic characteristics and prospecting significance of the Dounan manganese ore belt in Southeast Yunnan. Miner Depos 29:35–36 (in Chinese)

Banwart SA (1999) Reduction of iron (III) minerals by natural organic matter in groundwater. Geochim Cosmochim Acta 63:2919–2928

Berner RA (1981) Authigenic mineral formation resulting from organic matter decomposition in modern sediments. Fortschr Miner 59:117–135

Coey JMD, Schindler DW, Weber F (1974) Iron compounds in lake sediments. Can J Earth Sci 11:1489–1493

DeBaar HJW (1991) On cerium anomalies in the Sargasso sea. Geochim Cosmochim Acta 55:2981–2983

Du QD, Yi HS, Hui B, Li SJ, Xia GQ, Yang W, Wu XF (2013) Recognition, genesis and evolution of manganese ore deposits in southeastern China. Ore Geol Rev 55:99–109

Edwards BD (1985) Bioturbation in a dysaerobic, bathyal basin: California borderland. In: Curran HA (ed) Biogenic structures: their use in interpreting depositional environments, vol 35. Special Publications - SEPM, London, pp 309–331

Hilton J, Long GJ, Chapman JS, Lishman JP (1986) Iron mineralogy in sediments. A Mossbauer study. Geochim Cosmochim Acta 50:2147–2151

Hou BH (1994) Primary braunite in Triassic sedimentary manganese deposits of Dounan, Yunnan, China. Ore Geol Rev 9(3):219–239

Hou ZL, Xue ZY, Huang JS, Lin YH et al (1997) The Manganese deposits around the Yangtze platform. Metallurgical Industry Press, Beijing, pp 1–364 (in Chinese with English abstract)

Hu XY (2009) Determine themajor element concentrations of carbonate rocks using X-ray fluorescence spectrometry. Acta Miner Sin 598(S):597 (in Chinese)

Huang JH, Zhu KJ, Wang KJ, Wang SB, Zhu ZS (1996) Outline of marine Mn deposit in the South China. Contr Geol Miner Resour 11(3):9–17 (in Chinese with English abstract)

Jones B, Marning DAC (1994) Comparison of geochemical indices used for the interpretation of palaeoredox conditions in mudrocks. Chem Geol 1:111–129

Klein RT, Lohmann KC, Thayer CW (1996) Sr/Ca and ^{13}C/^{12}C ratios in skeletal calcite of MytiZus trossulus: covariation with metabolic rate, salinity, and carbon isotopic composition of seawater. Geochim Cosmochim Acta 60:4207–4221

Konhauser KO, Newman DK, Kappler A (2005) The potential significance of microbial Fe(III) reduction during deposition of Precambrian banded iron formations. Geobiology 3(3):167–177

Krauskopf KB (1957) Separation of manganese from iron in sedimentary process. Geochim Cosmochim Acta 2:61–84

Kubo K, Isozaki Y, Matsuo M (1996) Color of bedded chert and redox condition of depositional environment: ^{57}Fe Mössbauer spectroscopic study on chemical state of iron in Triassic deep-sea pelagic chert. J Geol Soc Jpn 102:40–48 (in Japanese with English abstract)

Kuno A, Matsuo M, Takano B (1998) Mössbauer spectroscopic study on vertical distribution of iron components in estuarine sediments collected from Tama River in Tokyo. Hyperfine Interact C3:328–331

Li SJ, Yi HS, Ma X, Xia GQ, Rong JF, Da XJ (2009) Sedimentary facies of the manganese-bearing strata in the Falang Formation, southeastern Yunnan. Sediment Geol Tethyan Geol 29(2):33–38 (in Chinese with English abstract)

Liu et al (1984) Typical deposit research report of Dounan manganese deposits, Yanshan County, Yunnan Province. Geol Miner Bur Yunnan Prov 86:1–106 (in Chinese)

Liu HJ, Xue YZ (1999) Sedimentology of Triassic Dounan-type manganese deposits, western margin, Yangtze platform, China. Ore Geol Rev 15:165–176

Liu RF, Tian BK, Shi ZZ, Hao RX, Li HC (1988) Geochemical characteristics of the Mn bearing-Falang formation in the Southeast Yunnan Province. Contr Geol Miner Resour Res 3(4):1–19 (in Chinese with English abstract)

Luo CX, Du ZY (1992) Lithofacies palaeogeography and ore-forming condition of main ore-bearing strata of the middle to late Triassic manganese resources at South margin of the upper Yangtze. Bull Chengdu Inst Geol Miner Resour Chin Acad Geol Sci 16:137–159

Manning PG, Ash LA (1979) Mössbauer spectral studies of pyrite, ferric and high-spin ferrous distributions in sulfide rich sediments from Moira Lake, Ontario. Can Miner 17:111–115

Matsuo M, Takano B, Sugimori K (1996) ^{57}Fe Mossbauer spectroscopic study of estuarine sediments taken from the Tama River in Tokyo. In: II Nuovo Cimento (Conf. Proc.), vol 50, pp 757–760

Morris RC, Horwitz RC (1983) The origin of the iron-formation-rich Hamersley group of western Australia—deposition on a platform. Precambr Res 21:273–297

Murray RW, Buchholtzten Brink MR, Jones DL, Gerlach DC, Price Russ III (1990) Rare earth elements as indicators of different marine depositional environments. Geology 18:268–271

Qi L, Hu JD, Conrad G (2000) Determination of trace elements in granites by inductively coupled plasma mass spectrometry. Talanta 51(3):507–513

Rasmussen B, Krape B, Meier DB (2014) Replacement origin for hematite in 2.5 Ga banded iron formation: evidence for postdepositional oxidation of iron-bearing minerals. Geol Soc Am Bull 126:438–446

Roy S (2006) Sedimentary manganese metallogenesis in response to the evolution of the Earth system. Earth Sci Rev 77:273–305

Sholkovitz ER, Schneider DL (1991) Cerium redox cycles and rare earth elements in the Sargasso Sea. Geochim Cosmochim Acta 55:2737–2743

Stevens JG, Khasanov AM, Miller JW, Pollak H, Li Z (eds) (1998) In: Mössbauer mineral handbook, Mössbauer effect data centre. University of North Carolina, Asheville, p 527

Su JH (1983) Dounan manganese deposit: a braunite deposit of sedimentary origin. Bull Inst Miner Depos Chin Acad Geol Sci 4:3–49 (in Chinese with English abstract)

Sun S, Li YL (2017) Geneses and evolutions of iron-bearing minerals in banded iron formations of > 3760 to ca. 2200 million-year-old: constraints from electron microscopic, X-ray diffraction and Mössbauer spectroscopic investigations. Precambr Res 289:1–17

Sun S, Konhauser KO, Kappler A, Li YL (2015) Primary hematite in Neoarchean to Paleoproterozoic oceans. Geol Soc Am Bull 127:850–861

Tang YF, Yi HS (2011) Mineral phase changes and depositional model of sedimentary manganese deposits in Dounan area of southeastern Yunnan. Geol China 38(2):451–461 (in Chinese with English abstract)

Tribovillard N, Algeo TJ, Lyonsc T, Riboulleau A (2006) Trace metals as paleoredox and paleoproductivity proxies: an update. Chem Geol 232:12–32

Tuccillo MA, Cozzarelli IM, Herman JS (1999) Iron reduction in the sediments of a hydrocarbon-contaminated. Appl Geochem 14:655–667

Tyson RV, Pearson TH (1991) Modern and ancient continental shelf anoxia: an overview. In: Tyson RV, Pearson TH (eds) Modern and ancient continental shelf anoxia, vol 58. Geological Society Special Publications, London, pp 1–26

Waander FB, Waanders Silva LO, Saikia BK (2017) The use of Mossbauer spectroscopy in environmental research. Hyperfine Interact 238:52

Wedepohl KH (1971) Environmental influences on the chemical composition of shales and clays. In: Ahrens LH, Press F,

Runcorn SK, Urey HC (eds) Physics and chemistry of the earth. Pergamon, Oxford, pp 305–333

Wedepohl KH (1991) The composition of the upper Earth's crust and the natural cycles of selected metals. In: Merian E (ed) Metals and their compounds in the environment. VCH-Verlagsge-sellschaft, Weinheim, pp 3–17

Wignall PB (1994) Black shale. Clarendon Press, Oxford, pp 1–127

Wu YL, Zhu HF (1994) Triassic lithofacies palaeogeography and mineralization in southern China. Geological Publishing House, Beijing, pp 99–103 **(in Chinese)**

Xia GQ, Yi HS, Li SJ, Wu XF (2010) Research on manganese—accumulation features in Middle Triassic Ladinian sedimentary system and sequence stratigraphic framework, Southeast Yunnan. Geol Rev 56(5):703–709 **(in Chinese with English abstract)**

Zheng RC, Zhang JQ (1991) Gravity flow manganese deposits and their sedimentary environments in Middle Triassic from Dounan, Southeast Yunnan. Chengdu Coll Geol 18(4):65–75 **(in Chinese)**

Zheng GD, Takano B, Kuno A, Katsuo M (2001) Iron speciation in modern sediment from Erhai lake, southwestern China: redox condition in an ancient environment. Appl Geochem 16:1201–1203

Zheng GD, Fu BH, Takahashi Y, Kuno A, Matsuo M, Zhang JD (2010) Chemical speciation of redox sensitive elements during hydrocarbon leaching in the Junggar Basin, Northwest China. J Asian Earth Sci 39:713–723

Zhong JT (1986) Metallogeny of the Dounan manganese deposit. Geol Rev 32(6):583–588 **(in Chinese with English abstract)**

Zhu XK, Peng QY, Zhang RB, An ZZ, Zhang FF, Yan B, Li J, Gao ZF, Tan Y, Pan W (2013) Geological and geochemical characteristics of the Daotuo super-large manganese ore deposit at Songtao County in Guizhou Province. Acta Geol Sin 87(09):1335–1348 **(in Chinese with English abstract)**